Supporting Information for

Polyphosphide anion-mediated simultaneous P, Au co-alloying with Pd for anti-poisoning formic acid oxidation

Yilan Chen, Jian Dong, Shuke Huang, Jun Li, Chenyang Zhao*

[a] College of Chemistry and Environmental Engineering, Shenzhen University, Shenzhen 518071, China.

E-mails: cyzhao@szu.edu.cn (Chenyang Zhao)

Experimental

Materials and reagents

Ethanol (C_2H_5OH, 99.7%) was purchased from Guangdong Guanghua Sci-Tech Co., Ltd. Palladium(Ⅱ) acetylacetonate (Pd $(AcAc)_2$, Pd≥34.7 wt.%) was purchased from Innochem Chemical Reagent Company. Red phosphorus (98.5%), potassium ethoxide (KOEt, 98.5%), 1,2-dimethoxyethane (DME, 99%), perchloric acid ($HClO_4$, 99.999%) and formic acid (AR, 88%) were purchased from Aladdin Chemical Reagent Company. Tetrahydrofuran (THF, 99%) and XC-72 conductive carbon black were purchased from Meryer Chemical Reagent Company. Chloroauric acid was purchased from Innochem Chemical Reagent Company. Commercial 10% Pd/C was purchased from Laajoo Chemical Reagent Company. The water used throughout all experiments was ultrapure water purified through a UPW system with resistance of 18.25 MΩ cm^{-1}.

Synthesis of soluble polyphosphide anions

All manipulations with air- and moisture-sensitive compounds were performed in an Ar-filled glovebox. Solid potassium ethoxide (KOEt, 400 mg) was dissolved in 15 mL of DME/THF (1:1 in volume) and red P (20 mg) was then added to the solution. After stirring at 85 ^oC for 2 hours, the resulting bright-orange suspension was centrifugalized, and the dark-red residue was dissolved in anhydrous EtOH to form a dark-red P_n^- solution.

Synthesis of P-PdAu

P-PdAu was synthesized through a one-pot approach, and the specific steps are as follows. First, 20 mg of carbon black (XC-72R) was dispersed in 20 mL of DMF under sonication for 40 min. Then, x mg (x= 5.05, 9.87, 13.7, 14) of palladium acetylacetonate and y μL (y=162.5, 79, 12, 7.5) of chloroauric acid were dissolved in the suspension. 5 mL of P_n^- solution was then slowly added. The reaction was kept in an Ar-filled glovebox under room temperature for 12h under stirring. Finally, the black solid was collected by centrifugation and washed with water, ethanol and acetone each 3 times. The samples are marked as P-Pd_1Au_1, P-Pd_4Au_1, P-$Pd_{40}Au_1$ and P-$Pd_{60}Au_1$ respectively based on the feeding molar ratio of Pd:Au. For comparison, P-Pd was also prepared in a similar way, but without the addition of chloroauric acid.

Electrochemical measurements

The electrochemical measurements of the catalysts were performed on a CHI660E electrochemical workstation at room temperature. A three-electrode system was used with a Pt wire as the counter electrode, a saturated calomel electrode (SCE) as the reference electrode, and a glassy carbon rotating disk electrode (GC-RDE, geometric area = 0.196 cm^2) as the working electrode. To prepare the catalyst ink, 2.5 mg of catalyst was dispersed in 1 mL mixture of water (900 μL), isopropanol (80 μL), and Nafion dispersion (5 wt.%, 20 μL) by sonication. 10 μL of catalyst ink was dropped onto the GC-RDE and dried, resulting in a 5 μg metal loading (based on the mass of Pd and Au). The sample was first activated by scanning between -0.26 and 0.91 V (*vs.*

SCE) at 50 mV s^{-1} in Ar-saturated 0.1 M $HClO_4$ solution for 50 cycles and then subjected to the cyclic voltammetry (CV) and polarization tests.

The CO stripping test was performed in a mixture of 0.1 M $HClO_4$ and 0.05 M HCOOH. Keeping the electrode potential at 0.01 V (*vs.* SCE), CO was first bubbled for 15 min, followed by Ar bubbling for 25 min to remove the excess CO. The CO striping curves were then obtained by scanning between -0.27 and 0.89 V at 20 mV s^{-1}. Assuming a value of 420 μC cm^{-2} for a saturated CO monolayer on the Pd surface, the number of active sites (n), electrochemical active specific surface area (ECSA) and turnover frequency (TOF) were calculated on basis of the CO stripping charges (Q_{CO}) with the following equations:

$$n = Q_{CO}/2Fm$$

$$ECSA = Q_{CO}/(m \times 420\ \mu C\ cm^{-2})$$

$$TOF = I/(2Fnm)$$

where m is the mass loading of Pd based on the ICP results and I is the polarization current (A). The factor 2 is the number of electrons transferred per HCOOH molecule.

Characterization

The morphology of the samples was investigated via transmission electron microscope (TEM, JEOL-F200, 200 kV). The microstructure was analyzed by spherical aberration corrected high-angle annular dark field scanning transmission

electron microscope (HAADF-STEM, FEI Titan Cubed Themis G2 30). X-ray diffraction analysis (XRD) were performed on Rigaku Mini Flex 600 with Cu Kα radiation (λ=1.5418Å). The measurements were conducted at a scan rate of 1.0°/min between 30-90°. The elemental valence analysis was performed by X-ray photoelectron spectroscopy (XPS, Thermo Electron, Al Kα X-rays, 1486.6 eV). The compositions of the samples were tested by inductively coupled plasma mass spectrometry (ICP-MS, Avio 2000).

Theoretical calculation

We have employed the Vienna Ab Initio Package (VASP)[1, 2] to perform all the density functional theory (DFT) calculations within the generalized gradient approximation (GGA) using the PBE formulation.[3] We have chosen the projected augmented wave (PAW) potentials to describe the ionic cores and taken valence electrons into account using a plane wave basis set with a kinetic energy cutoff of 400 eV.[4, 5] Partial occupancies of the Kohn−Sham orbitals were allowed using the Gaussian smearing method and a width of 0.05 eV. The electronic energy was considered self-consistent when the energy change was smaller than 10^{-5} eV. A geometry optimization was considered convergent when the force change was smaller than 0.02 eV/Å. Grimme's DFT-D3 methodology was used to describe the dispersion interactions.[6]

The equilibrium lattice constant of fcc unit cell was optimized to be a=3.886 Å using a 10×10×10 Monkhorst-Pack k-point grid for Brillouin zone sampling. We then use it

to construct a pristine Pd(111) surface model with p(3×2√3) periodicity in the x and y directions and 4 atomic layers in the z direction separated by a vacuum layer in the depth of 15 Å in order to separate the surface slab from its periodic duplicates. This surface model contains 48 Pd atoms. During structural optimizations, a 2×2×1 k-point grid in the Brillouin zone was used for k-point sampling, and the bottom two atomic layers were fixed while the top two were allowed to relax.

The adsorption energy (E_{ads}) of adsorbate A was defined as

$$E_{ads} = E_{A/surf} - E_{surf} - E_{A(g)}$$

where $E_{A/surf}$, E_{surf} and $E_{A(g)}$ are the energy of adsorbate A adsorbed on the surface, the energy of clean surface, and the energy of isolated A molecule in a cubic periodic box with a side length of 20 Å and a 1×1×1 Monkhorst-Pack k-point grid for Brillouin zone sampling, respectively. The free energy of a gas phase molecule or an adsorbate on the surface was calculated by the equation G = E + ZPE − TS, where E is the total energy, ZPE is the zero-point energy, T is the temperature in kelvin (298.15 K is set here), and S is the entropy.

Fig. S1. An optical photograph of the P_n^- in anhydrous ethanol.

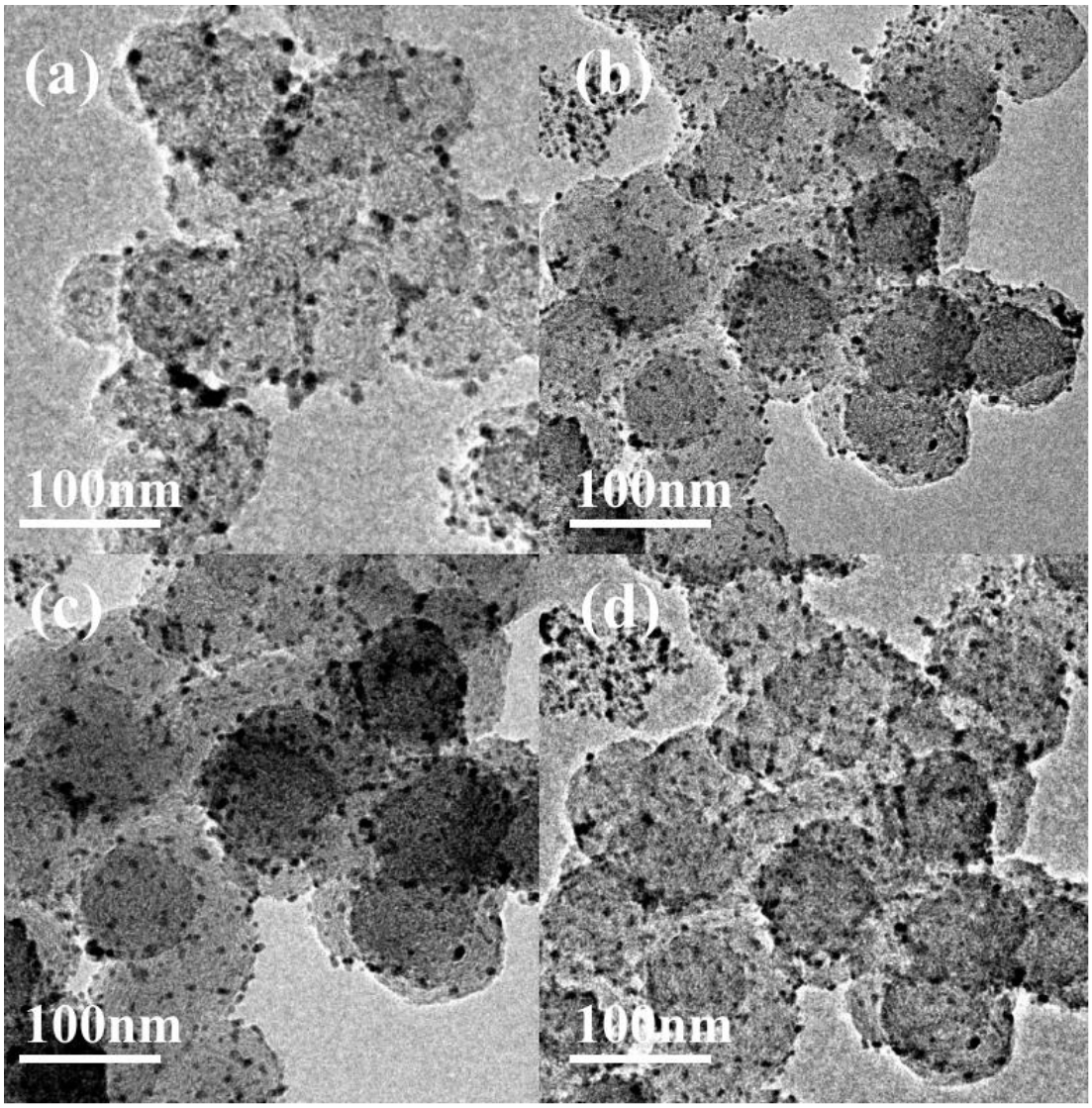

Fig. S2. TEM images of (a) P-Pd_1Au_1,(b) P-Pd_4Au_1, (c) P-$Pd_{40}Au_1$, (d) P-$Pd_{60}Au_1$.

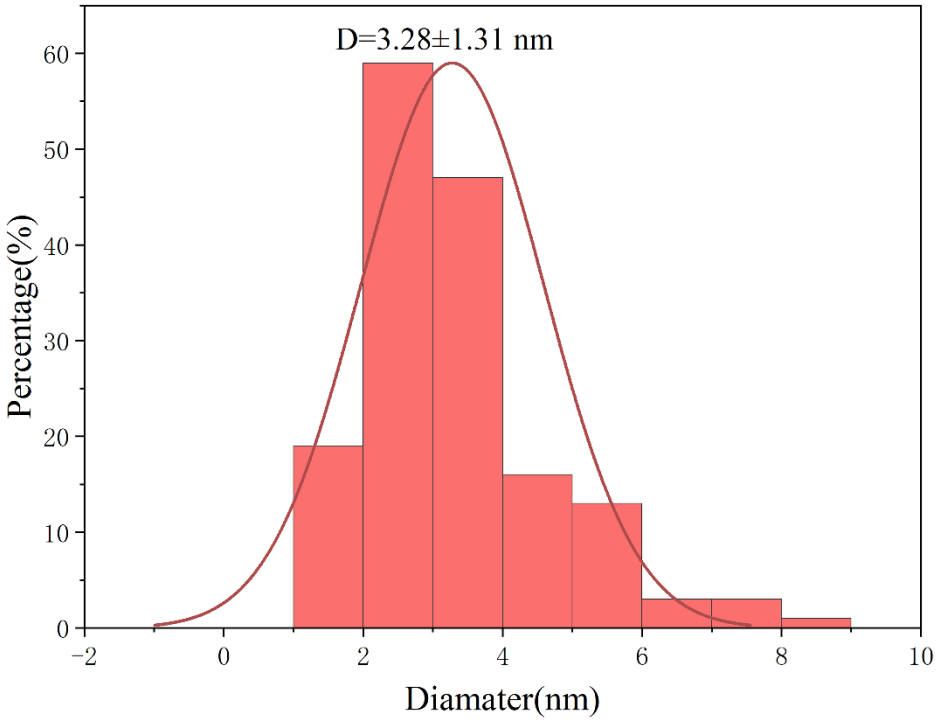

Fig. S3. Particle size distribution of P-$Pd_{40}Au_1$.

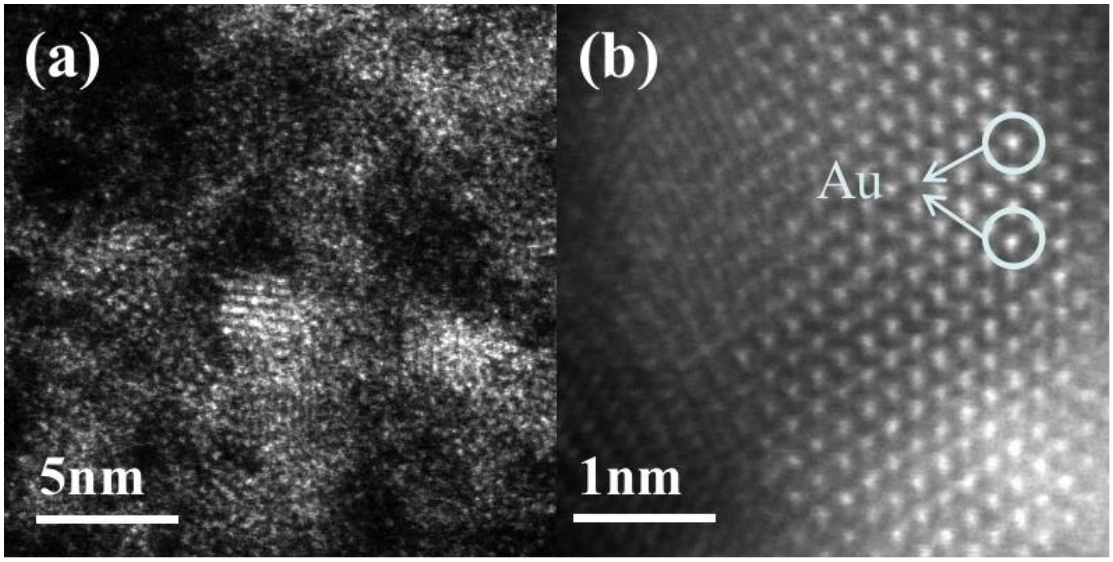

Fig. S4. HAADF-STEM images of P-$Pd_{40}Au_1$.

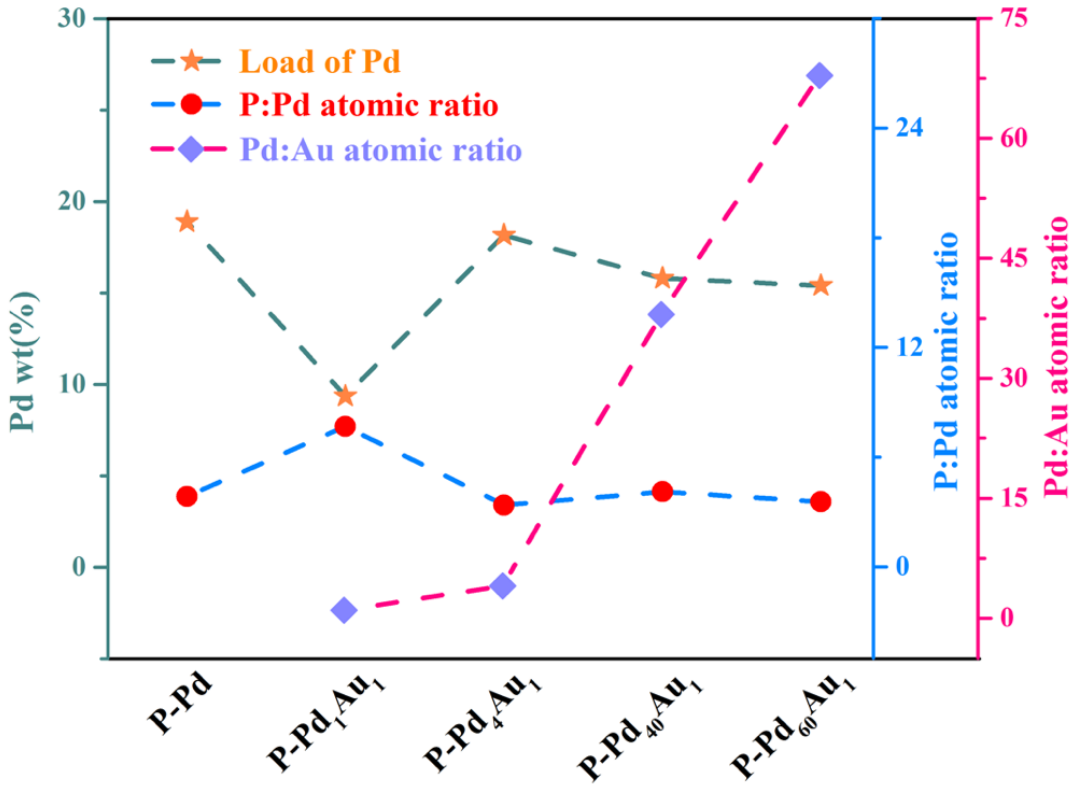

Fig. S5. The Pd content, atomic ratio of P to Pd, and atomic ratio of Pd to Au of P-Pd, P-$Pd_{60}Au_1$, P-$Pd_{40}Au_1$, P-Pd_4Au_1, and P-Pd_1Au_1 determined by ICP.

The specific compositions of the samples were measured by ICP. As shown in Fig. S5, the Pd contents of the samples are around 20 wt% expect for P-Pd_1Au_1, consistent with the molar ratio of metal precursors. The atomic ratio of Pd to Au ranges from ~1 (P-Pd_1Au_1) to ~68 (P-$Pd_{60}Au_1$) with the decrease of Au content. The atomic ratio of P to Pd is around 4 for P-Pd, P-Pd_4Au_1, P-$Pd_{40}Au_1$ and P-$Pd_{60}Au_1$. The slight higher atomic ratio of P to Pd in P-Pd_1Au_1 is caused by the excessive Au substitution. The ICP results manifest high reliability of this P_n^- mediated P-doping/reduction process.

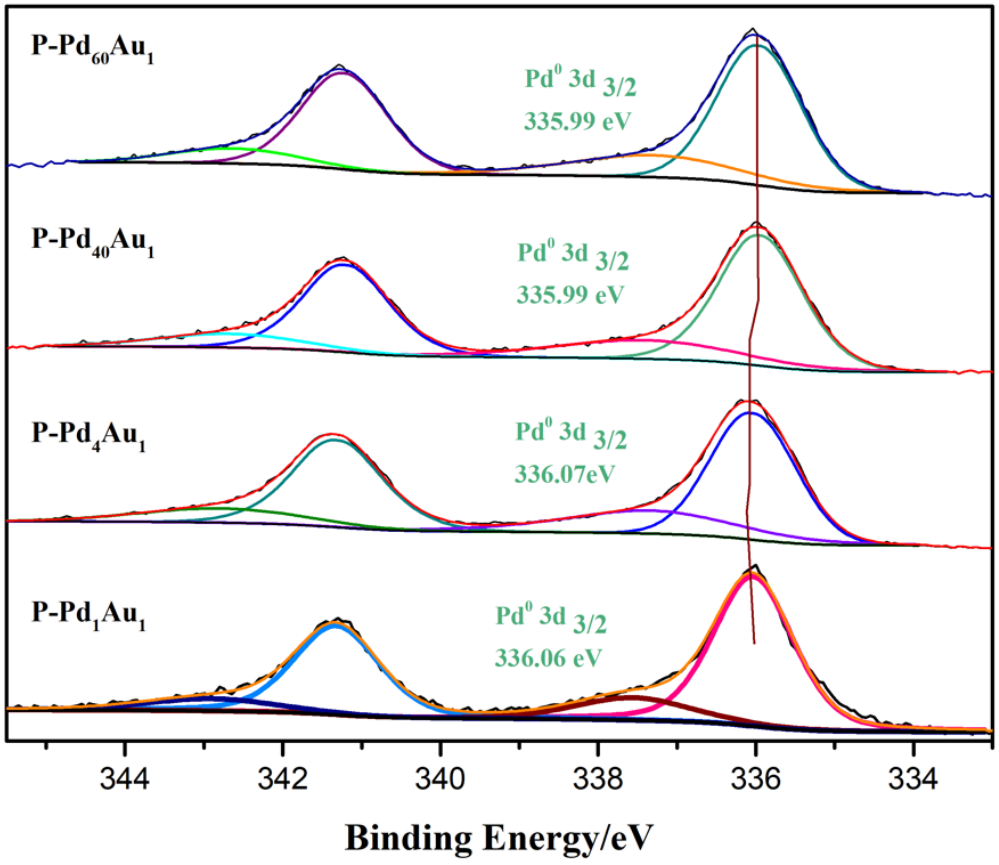

Fig. S6. XPS spectra of Pd 3d orbitals of P-$Pd_{60}Au_1$, P-$Pd_{40}Au_1$, P-Pd_4Au_1, and P-Pd_1Au_1.

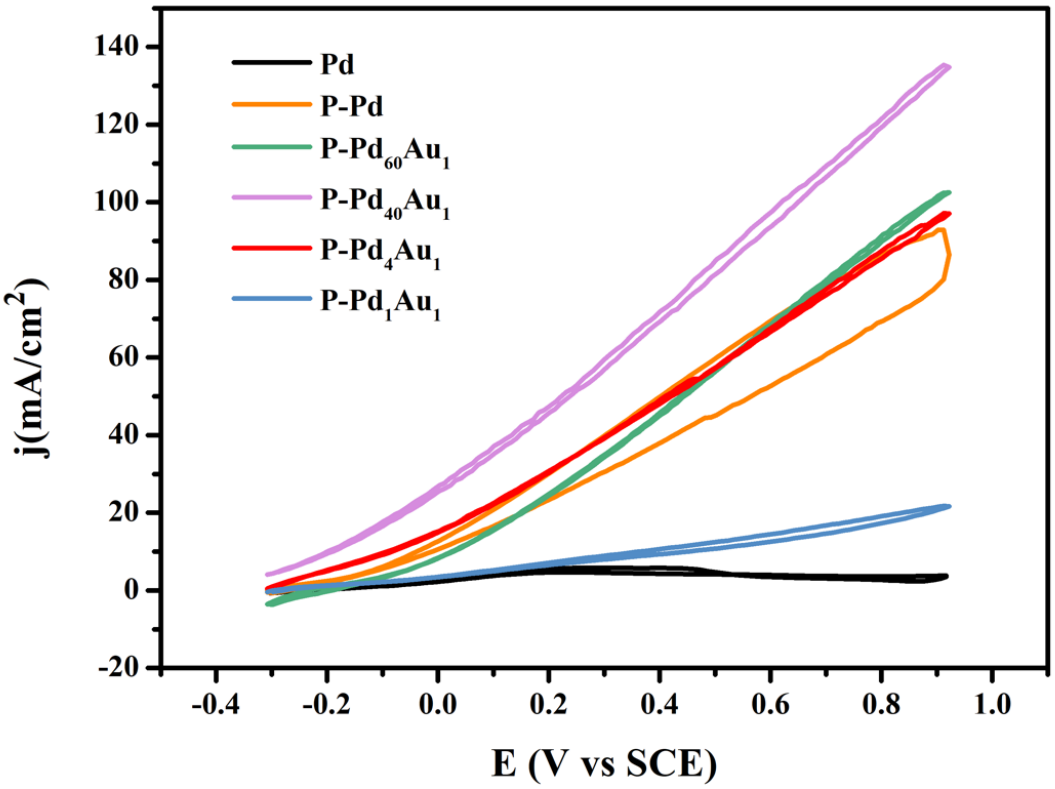

Fig. S7. FAOR polarization curves of the P-PdAu, P-Pd and Pd/C recorded in an Ar-saturated mixed solution of 0.1 M $HClO_4$ and 2 M HCOOH (normalized by geometric area of electrode).

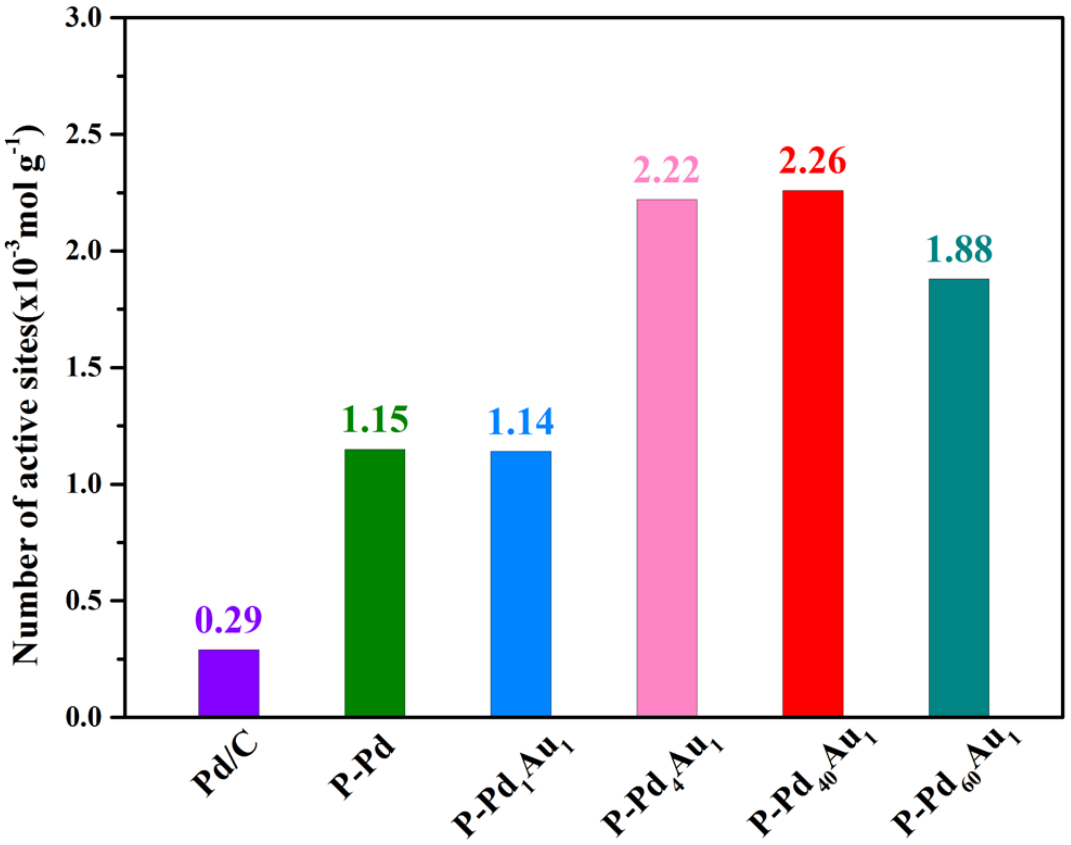

Fig. S8. Number of active sites of P-PdAu, P-Pd and commercial Pd/C.

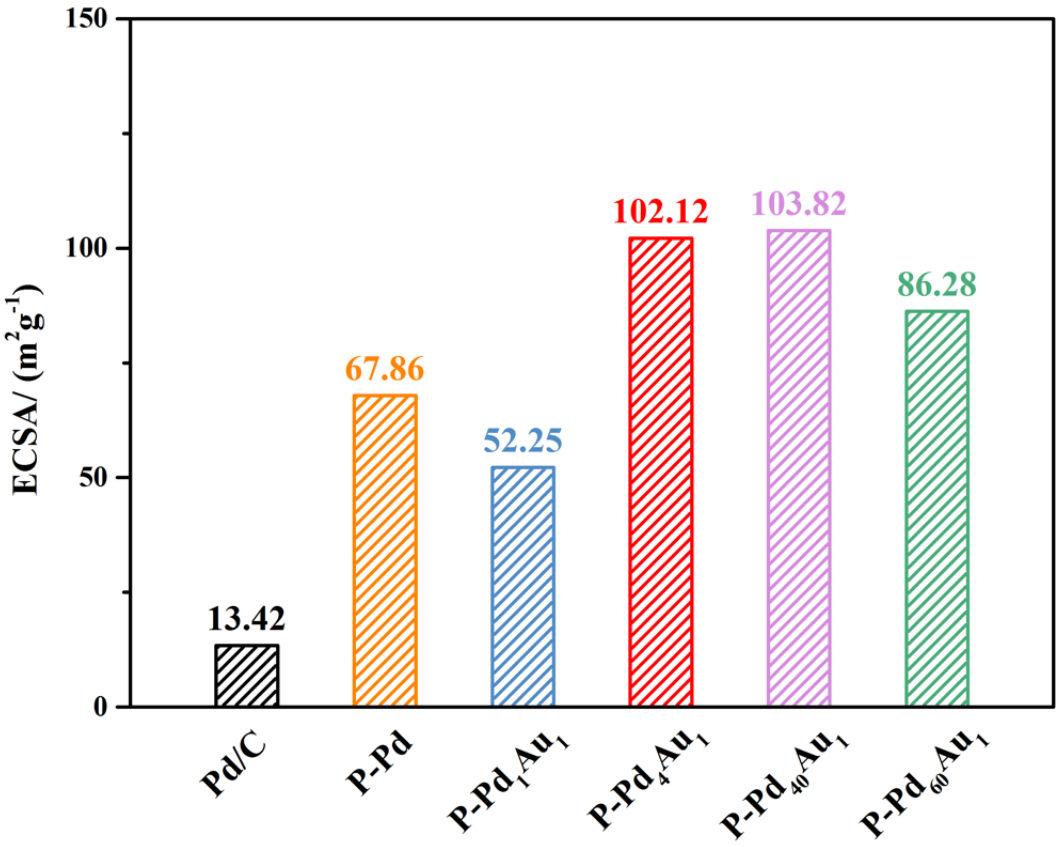

Fig. S9. ECSA of P-PdAu, P-Pd and commercial Pd/C.

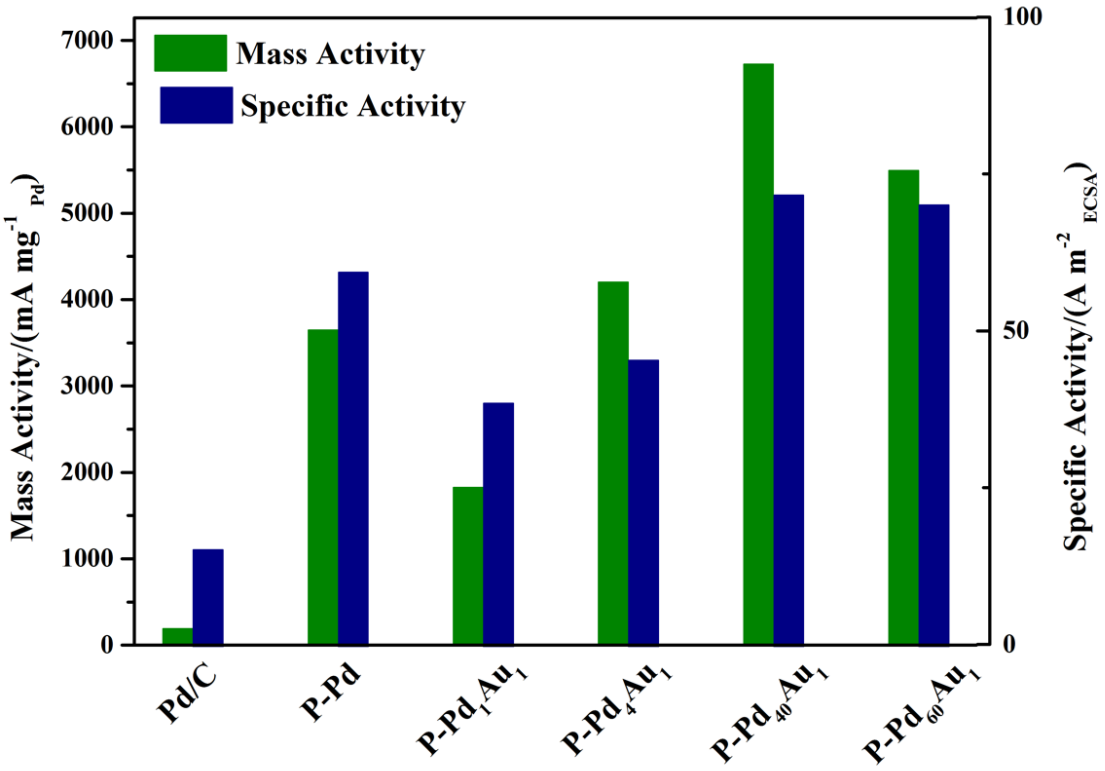

Fig. S10. The mass activities and specific activities of P-PdAu, P-Pd and commercial Pd/C.

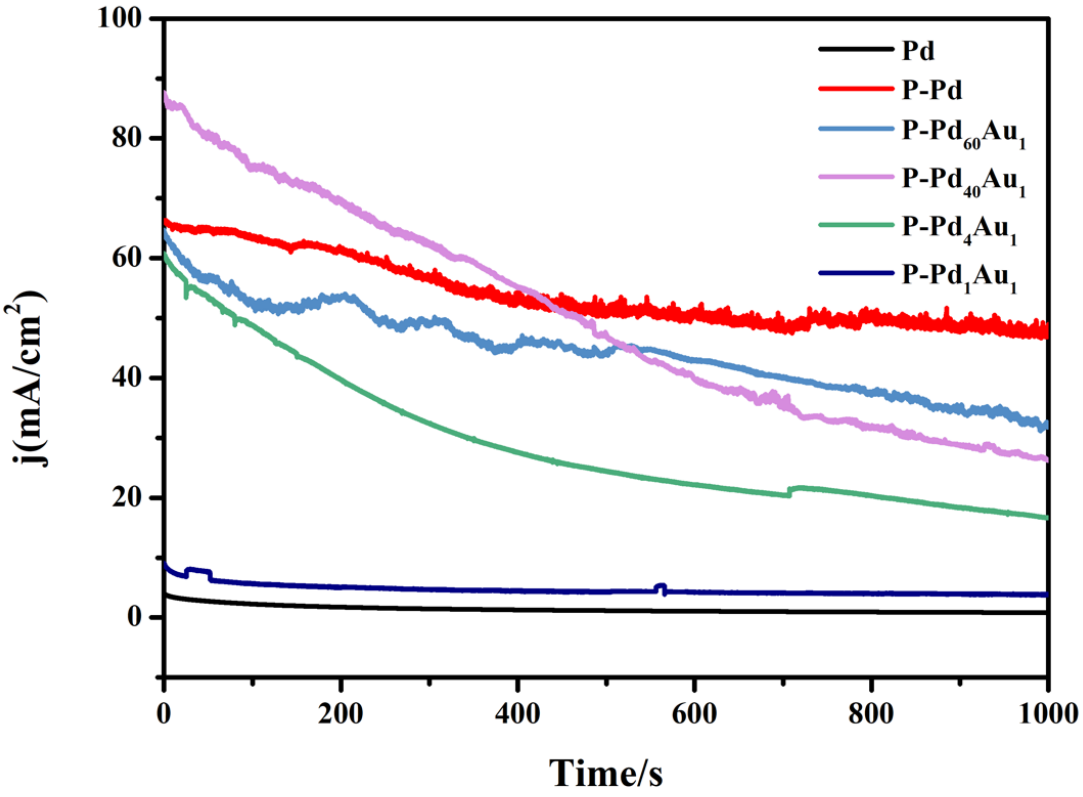

Fig. S11 1000s stability test of the P-PdAu, P-Pd and Pd/C at a sweep rate of 50 mV/s in an Ar-saturated mixed solution of 0.1 M $HClO_4$ and 2 M HCOOH (normalized by geometric area of electrode).

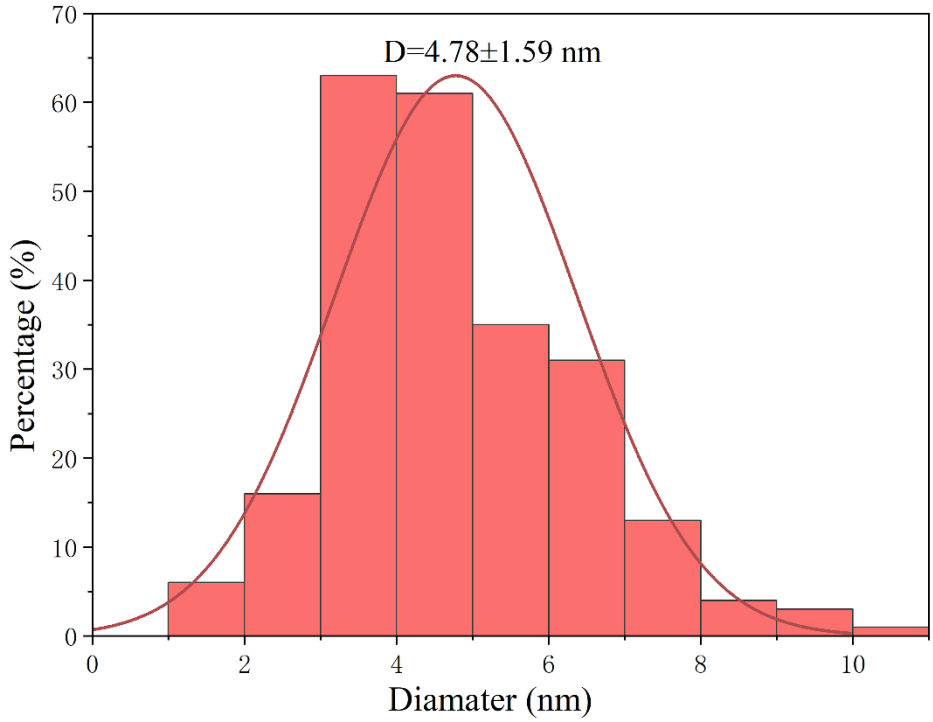

Fig. S12. Particle size distribution of P-$Pd_{40}Au_1$ after the stability test.

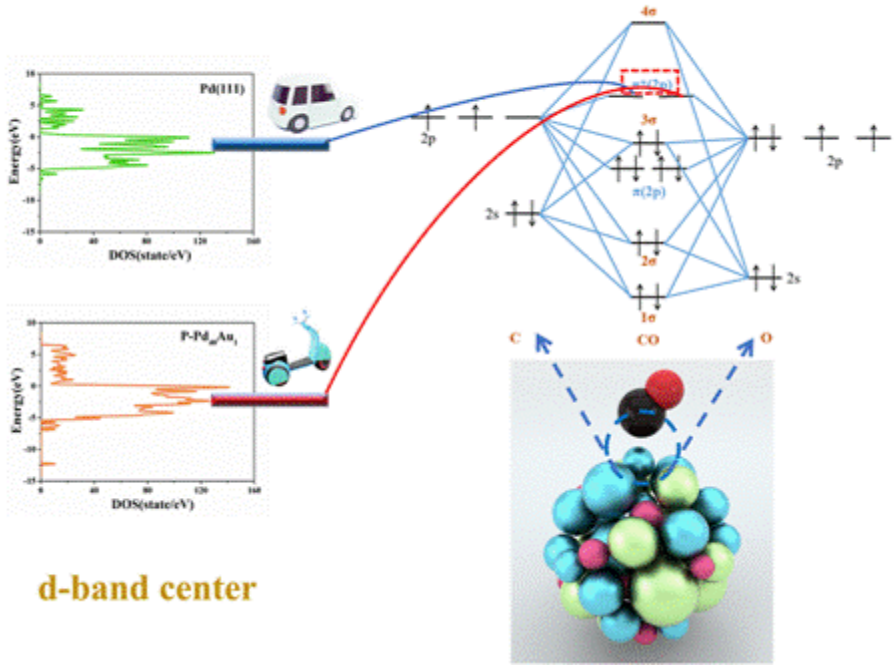

Fig. S13. Density of states of P-$Pd_{40}Au_1$ and Pd and molecular orbital of CO.

Fig. S14. The decomposition pathway of formic acid molecule on P-$Pd_{40}Au_1$ model. Color code: Gray, pink, yellow, brown, red and mauve represent Pd, P, Au, C, O and H respectively.

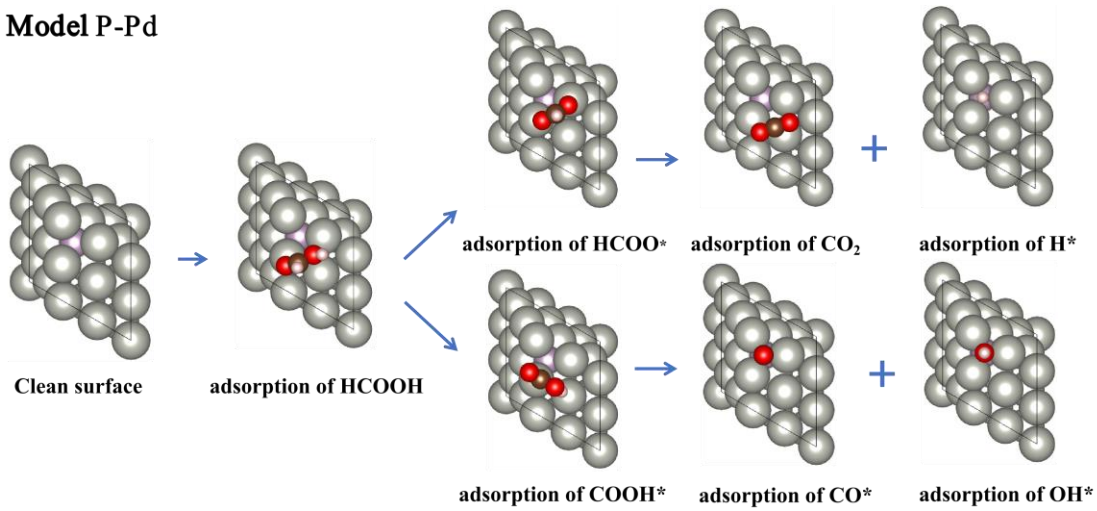

Fig. S15. The decomposition pathway of formic acid molecule on P-Pd model. Color code: Gray, pink, brown, red and mauve represent Pd, P, C, O and H respectively.

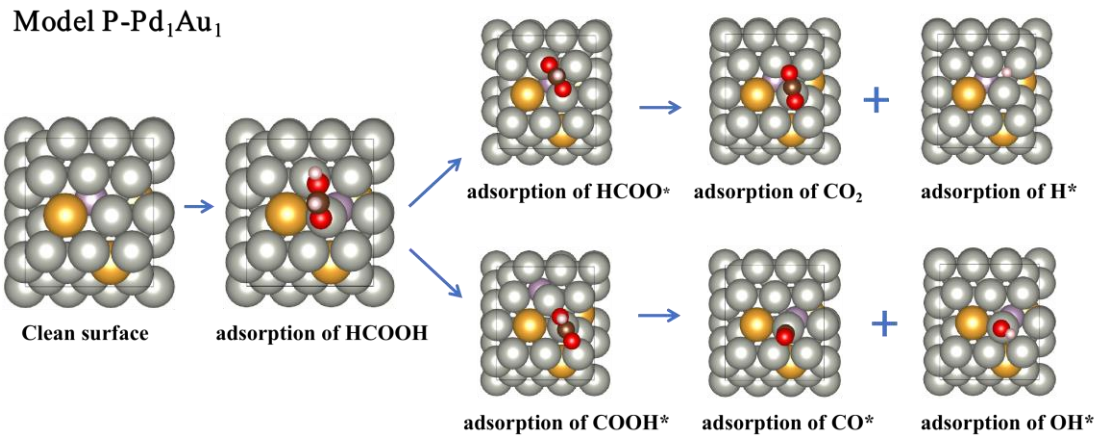

Fig. S16. The decomposition pathway of formic acid molecule on P-Pd_1Au_1 model. Color code: Gray, pink, yellow, brown, red and mauve represent Pd, P, Au, C, O and H respectively.

Table S1 The Pd, Au and P contents of the samples.

	P-Pd	**P-Pd$_1$Au$_1$**	**P-Pd$_4$Au$_1$**	**P-Pd$_{40}$Au$_1$**	**P-Pd$_{60}$Au$_1$**
Pd (wt %)	18.9	9.36	18.16	15.8	15.4
Au (wt %)	\	9.36	4.46	0.42	0.23
P (wt %)	0.73	0.72	0.62	0.65	0.55

Table S2. Comparison of Q_{CO}, ECSA, n and TOF of P-PdAu, P-Pd and commercial Pd/C.

Catalysts	**Q_{CO} (m C)**	**ECSA ($m^2 g^{-1}$)**	**Number of active sites (10^{-3} mol g^{-1})**	**TOF at the 0.8V (s^{-1})**
Commercial Pd/C	0.28	13.42	0.29	2.52
P-Pd	1.42	67.87	1.15	11.91
P-Pd_1Au_1	0.51	52.25	1.14	7.34
P-Pd_4Au_1	1.95	102.12	2.22	8.831
P-$Pd_{40}Au_1$	1.72	103.82	2.26	13.87
P-$Pd_{60}Au_1$	1.40	86.28	1.88	13.14

References

1. Kresse, G.; Furthmüller, J. Efficiency of Ab-Initio Total Energy Calculations for Metals and Semiconductors Using a Plane-Wave Basis Set. Comput. Mater. Sci. 1996, 6, 15−50.
2. Kresse, G.; Furthmüller, J. Efficient Iterative Schemes for Ab Initio Total-Energy Calculations Using a Plane-Wave Basis Set. Phys. Rev. B 1996, 54, 11169−11186.
3. Perdew, J. P.; Burke, K.; Ernzerhof, M. Generalized Gradient Approximation Made Simple. Phys. Rev. Lett. 1996, 77, 3865−3868.
4. Kresse, G.; Joubert, D. From Ultrasoft Pseudopotentials to the Projector Augmented-Wave Method. Phys. Rev. B 1999, 59, 1758-1775.
5. Blöchl, P. E. Projector Augmented-Wave Method. Phys. Rev. B 1994, 50, 17953−17979.
6. Grimme, S.; Antony, J.; Ehrlich, S.; Krieg, H. J. Chem. Phys. 2010, 132, 154104.